Theory of 360° domain walls in thin ferromagnetic films

C. B. Muratov[1,a)] and V. V. Osipov[2]
[1]*Department of Mathematical Sciences, New Jersey Institute of Technology, Newark, NJ 07102, USA*
[2]*Mission Critical Technologies, Inc., 2041 Rosecrans Avenue, Suite 225, El Segundo, California 90245, USA and Intelligent Systems Division, D&SH Branch, NASA Ames Research Center, MS 269-1, Moffett Field, California 94035, USA*

(Received 13 May 2008; accepted 19 June 2008; published online 11 September 2008)

An analytical and computational study of 360° domain walls in thin uniaxial ferromagnetic films is presented. The existence of stable one-dimensional 360° domain wall solutions both with and without the applied field is demonstrated in a reduced thin film micromagnetic model. The wall energy is found to depend rather strongly on the orientation of the wall and the wall width significantly grows when the strength of the magnetostatic forces increases. It is also shown that a critical reverse field is required to break up a 360° domain wall into a pair of 180° walls. The stability of the 360° walls in two-dimensional films of finite extent is demonstrated numerically and the stability with respect to slow modulations in extended films is demonstrated analytically. These domain wall solutions are shown to play an important role in magnetization reversal. In particular, it is found that the presence of 360° domain walls may result in nonuniqueness of the observed magnetization patterns during repeated cycles of magnetization reversal by pulsed fields. © *2008 American Institute of Physics*. [DOI: 10.1063/1.2970100]

I. INTRODUCTION

It is well known that domain structures often arise in real magnetic materials and determine many of their properties.[1–4] Of particular interest are the domain structures in thin magnetic metallic films which have been extensively investigated during the last two decades,[5–11] primarily in the context of giant magnetoresistance and magnetic tunnel junction devices.[4,12–16] Furthermore, spin-injection switching of the magnetization configuration in thin films with in-plane magnetization by electric current has been theoretically predicted[17,18] and observed experimentally in thin film multilayers.[19–21] In addition, thin magnetic films are the basis for the development of different types of magnetic memories including magnetoresistive random access memory.[4,16,22–25]

As a rule, the easy direction of anisotropy of thin metallic magnetic films lies in the film plane.[5,7–9] It is clear that the equilibrium state of an extended thin film with in-plane magnetization is a monodomain state because the magnetostatic energy, which tends to induce domain formation, is negligible in this case. Nevertheless, various magnetization structures, in particular, the so-called Néel walls, in which the magnetization rotates by 180° between the two directions of the easy axis are observed in the majority of thin films with in-plane magnetization.[2,7,8] Back in the beginning of the 1960s (Refs. 26–29) many authors noted that 360° domain walls and other more complicated winding magnetization structures also form very often in thin films in the process of magnetization reversal.[2,10,24,30–33] A typical scenario in which a 360° wall appears involves a passage of a Néel wall over a nonmagnetic impurity with a pinned Bloch line during magnetization reversal.[2,26–29,31,33] This scenario was confirmed by three-dimensional micromagnetic simulations of moderately thin films.[34] At the same time, 360° domain walls are also observed to form in the process of magnetization reversal in the absence of any apparent defects in the film.[2,24,30,33,35]

From the point of view of applications, 360° domain walls are a nuisance to avoid, since they generally complicate the process of magnetization switching and may reduce the reproducibility of the switching events. At the same time, the existence of stable 360° domain walls poses an intriguing possibility of using their topological characteristics to store information in magnetic storage devices. Nevertheless, despite the widespread appearance of 360° domain walls in thin ferromagnetic films and their potential undesirable or beneficial effect for the operation of thin film–based devices, to the best of our knowledge, there have been no systematic micromagnetic studies of these walls to date. In particular, the magnetization profiles in 360° walls, their stability, their dynamics under the action of an applied field have not been studied in detail. Even the question whether the observed 360° walls are stable magnetization structures or just long-lived metastable states has not been resolved yet.[2] At the same time, we believe that in order to properly interpret the experimental observations in the materials of interest for current technological applications and to propose new ones, one has to better understand the properties of magnetic winding structures and the role of their dynamics during switching in thin films.

In this paper we consider these urgent problems. We perform analytical and computational studies of a reduced micromagnetic model which is appropriate for thin films with in-plane easy axis. We prove numerically the existence of stable one-dimensional 360° domain wall solutions in the absence of the applied field in a broad range of the thin film parameter and wall orientations, as long as the wall makes a nonzero angle with the easy axis. We further demonstrate

a)Electronic mail: muratov@njit.edu.

that the 360° domain wall solutions persist in an applied field and that a finite reverse field is necessary to break them up. We further computationally investigate the stability (in the sense of dynamics, we do not consider the effect of thermal fluctuations here) of the 360° walls in two-dimensional films, using a novel numerical algorithm based on the application of optimal finite-difference grids[36] to thin film simulations, developed by us in Ref. 37. We argue that the wall motion in large samples must be described by an anisotropic mean-curvature flow. At the same time, both the applied and the stray fields may result in the wall breakup, leading to complicated magnetization reversal dynamics.

Our paper is organized as follows. In Sec. II, we introduce the reduced micromagnetic model which is the basis of the analysis and simulations that follow. In Sec. III, we describe the results of our analysis of the existence, properties, and stability of the 360° domain wall solutions. Also in Sec. III, we perform a variational study of the wall profiles and investigate the role of 360° domain walls in the magnetization reversal by pulsed fields. Finally, in Sec. IV we summarize our findings.

II. MODEL

We start with the Landau–Lifshitz–Gilbert equation,[2] which describes the dynamics of the magnetization vector $\mathbf{M}=(M_1,M_2,M_3)$ of fixed magnitude $|\mathbf{M}|=M_s$ in a ferromagnetic material,

$$\frac{\partial \mathbf{M}}{\partial t}=-\frac{g|e|}{2mc}\left(\mathbf{M}\times\mathbf{H}_{\text{eff}}+\frac{\alpha}{M_s}\mathbf{M}\times\mathbf{M}\times\mathbf{H}_{\text{eff}}\right),$$
$$\left.\frac{\partial \mathbf{M}}{\partial n}\right|_{\partial\Omega}=0. \tag{1}$$

Here, $\mathbf{M}=\mathbf{M}(\mathbf{r},t)$, with the position vector $\mathbf{r}=(x,y,z)$ lying in a three-dimensional domain Ω occupied by the material. This domain is assumed to be a film of thickness d and shape specified by a two-dimensional set D, i.e., $(x,y)\in D\subseteq\mathbb{R}^2$ and $0<z<d$ for all $(x,y,z)\in\Omega$. The factor $g|e|/(2mc)$ is the gyromagnetic ratio (we use cgs units here and below), α is a dimensionless parameter, and the last term in Eq. (1) specifies Neumann boundary conditions.

The first term in Eq. (1) governs the precession of the magnetization vector in the presence of the effective magnetic field $\mathbf{H}_{\text{eff}}$, and the second term introduces phenomenological damping. The effective field $\mathbf{H}_{\text{eff}}$ is determined self-consistently as

$$\mathbf{H}_{\text{eff}}=-\frac{\delta E}{\delta \mathbf{M}}, \tag{2}$$

where the energy functional $E[\mathbf{M}]$ is given by

$$E[\mathbf{M}]=\int_\Omega\left(-\frac{K}{2M_s^2}M_2^2+\frac{A}{2M_s^2}|\nabla\mathbf{M}|^2-\mathbf{H}\cdot\mathbf{M}\right)d^3\mathbf{r}$$
$$+\frac{1}{2}\int_{R^3}\int_{\mathbb{R}^3}\frac{\nabla\cdot\mathbf{M}(\mathbf{r})\,\nabla\cdot\mathbf{M}(\mathbf{r}')}{|\mathbf{r}-\mathbf{r}'|}d^3\mathbf{r}d^3\mathbf{r}', \tag{3}$$

where in the last term $\mathbf{M}$ is extended by zero to the whole space and the derivative is understood in the distributional sense. The energy in Eq. (3) consists of the anisotropy (first term), exchange (second term), external field (third term), and the magnetostatic (fourth term) contributions, with K and A being the respective material constants and $\mathbf{H}$ the applied field. For simplicity we assumed that the anisotropy is uniaxial in the film plane, other types of in-plane anisotropy can be treated similarly.

We are interested in the regime of thin films and moderately soft materials. For such films the model in Eqs. (1)–(3) can be considerably simplified under suitable assumptions on the magnitudes of the material constants and the film thickness.[37] These assumptions can be conveniently formulated in terms of the values of the exchange length $l=(A/4\pi M_s^2)^{1/2}$ and the Bloch wall thickness $L=(A/K)^{1/2}$, whose ratio defines the material's quality factor $Q=(l/L)^2$, with $Q\ll 1$ in a soft material. First of all, in order for the film to be considered thin, the thickness of the film should not exceed the exchange length: $d\lesssim l$ (more precisely, $d\lesssim 7l$ in the context of Néel walls[2,7,38]). On the other hand, while in a soft material $L\gtrsim l$, in a thin film it is still possible to have a balance $Ld/l^2\sim 1$. Such a balance is readily realized in thin metallic ferromagnetic films,[7] e.g., in 2-nm-thick cobalt films with $l=5$ nm and $Q=0.1$.

Under the above balance, let us introduce a dimensionless quantity which will play the role of a single effective film parameter in the considered regime,[37]

$$\nu=\frac{4\pi M_s^2 d}{\sqrt{AK}}=\frac{d}{l\sqrt{Q}}. \tag{4}$$

This parameter measures the strength of the magnetostatic interaction relative to both anisotropy and exchange in thin films. We note that in ultrathin ($d\ll l$) films consisting of only a few monolayers of the magnetic material with $Q\lesssim 1$, it is possible to make this parameter rather small. On the other hand, for soft materials ($Q\ll 1$) the parameter ν can also be relatively large, increasing with the film thickness. Nevertheless, the condition $d\lesssim l$ of validity of the thin film approximation, which by Eq. (4) is equivalent to $\nu\lesssim Q^{-1/2}$, may remain valid even for $\nu\gg 1$, as long as the film thickness is not too large compared to the exchange length.

When $Q\ll 1$ and ν is not too large, the magnetization $\mathbf{M}$ becomes independent of z and the out-of-plane component M_3 is strongly penalized.[37,39,40] Furthermore, if α is not too small, the effective dynamics becomes overdamped.[39–42] To write the obtained effective equation, let us introduce the rescaling (choosing L as the unit of length)

$$\mathbf{m}=\frac{\mathbf{M}}{M_s},\quad \mathbf{h}=\frac{M_s\mathbf{H}}{K},\quad \mathbf{r}\to\mathbf{r}\sqrt{\frac{A}{K}},\quad t\to t\frac{2mcM_s}{g|e|K} \tag{5}$$

and ignore the z-dependence of $\mathbf{m}$. Now $|\mathbf{m}|=1$ in Ω, and setting $\mathbf{m}\simeq(\tilde{\mathbf{m}},0)$, where $\tilde{\mathbf{m}}=\tilde{\mathbf{m}}(\mathbf{r},t)$ is a two-dimensional unit vector depending on time and position $\mathbf{r}\in D$ in the film, after some algebra we arrive at[39]

$$\frac{\partial \mathbf{m}}{\partial t} = -\left(\alpha + \frac{1}{\alpha}\right)\mathbf{m} \times \mathbf{m} \times \mathbf{h}_{\text{eff}}, \tag{6}$$

where $\mathbf{h}_{\text{eff}}=(\tilde{\mathbf{h}}_{\text{eff}},0)$, with the two-dimensional vector field $\tilde{\mathbf{h}}_{\text{eff}}$ given by[37]

$$\tilde{\mathbf{h}}_{\text{eff}} = (m_2 + h)\mathbf{e}_2 + \Delta \mathbf{m} + \frac{\nu}{4\pi} \nabla \int_D \frac{\nabla \cdot \mathbf{m}(\mathbf{r}')}{|\mathbf{r} - \mathbf{r}'|} d^2\mathbf{r}'. \tag{7}$$

Here $\Delta = \partial^2/\partial x^2 + \partial^2/\partial x^2$, $\mathbf{e}_2$ is the unit vector along the y-axis, and we assumed that $\mathbf{h}=(0,h,0)$ (in fact, most of our analysis is done in the absence of the applied field, $h=0$). Let us note that the last term in Eq. (7) can be expressed in terms of the Neumann-to-Dirichlet operator $(-\Delta)^{-1/2}$ associated with Laplace's equation in half-space,[43]

$$u = (-\Delta)^{-1/2} v \Leftrightarrow u(\mathbf{r}) = \frac{1}{2\pi} \int_{\mathbb{R}^2} \frac{v(\mathbf{r}')}{|\mathbf{r} - \mathbf{r}'|} d^2\mathbf{r}', \tag{8}$$

which can be thought of as the inverse square root of the negative Laplacian operator on the xy-plane. That is, we have simply

$$e^{-iq_1x - iq_2y}(-\Delta)^{-1/2} e^{iq_1x + iq_2y} = (q_1^2 + q_2^2)^{-1/2}. \tag{9}$$

Therefore, this operator can be easily computed in Fourier space.[43]

The obtained set of equations is most conveniently rewritten in terms of the angle θ between $\tilde{\mathbf{m}}$ and the easy axis. Setting $\tilde{\mathbf{m}}=(-\sin\theta, \cos\theta)$, we obtain an equation[37] which involves only one scalar unknown quantity θ,

$$\frac{\partial \theta}{\partial t} = \Delta\theta - \frac{1}{2}\sin 2\theta - h \sin\theta + \nu \cos\theta \frac{\partial \varphi}{\partial x} + \nu \sin\theta \frac{\partial \varphi}{\partial y}, \tag{10}$$

$$\varphi = \frac{1}{2}(-\Delta)^{-1/2}\left(\cos\theta \frac{\partial \theta}{\partial x} + \sin\theta \frac{\partial \theta}{\partial y}\right) + \text{boundary terms}, \tag{11}$$

where we absorbed the factor of $\alpha + \alpha^{-1}$ into the definition of time. Our analysis that follows will be based on this set of equations for θ. Note that this equation can be formally derived from Eq. (1) in the asymptotic limits $Q \to 0$ and $d \to 0$ simultaneously, with ν and α fixed.[37] Also note that for smaller values of the damping coefficient (when $\alpha \lesssim Q^{1/2}$) one can similarly obtain Eq. (10) with an extra term proportional to $\partial^2\theta/\partial t^2$ in the left-hand side.[44]

III. RESULTS

A. Preliminaries: The case of $\nu=0$ (neglecting magnetostatics)

We are now going to study the existence of 360° domain wall solutions of Eqs. (10) and (11), i.e., stationary solutions of these equations with or without applied field in a film of infinite extent, i.e., when $D=\mathbb{R}^2$. These solutions must satisfy some limit boundary conditions at infinity. To make the meaning of these boundary conditions more precise, it is instructive to consider a simplified version of Eq. (10) with the magnetostatic term neglected. Setting $\nu=0$ and $\partial\theta/\partial t = 0$ in Eq. (10), we get a nonlinear elliptic equation in $\mathbb{R}^2$,

$$\Delta\theta - \tfrac{1}{2}\sin 2\theta - h \sin\theta = 0. \tag{12}$$

This type of equations has been very well studied in the mathematical literature. In fact, it is now known that for $h>0$ the only "wall-like" solutions of Eq. (12) are one-dimensional fronts.[45] More precisely, any solution of Eq. (12) which is bounded between 0 and 2π and monotone in some direction must be essentially a function of one variable, i.e., there exists an angle α such that after rotating the coordinate system by this angle,

$$\xi = x \cos\alpha + y \sin\alpha, \qquad \eta = y \cos\alpha - x \sin\alpha, \tag{13}$$

the solution of Eq. (12) is a function of ξ only [of course, here and everywhere below there should be no confusion between the angle α and the damping coefficient in Eq. (1)]. Moreover, in the case of Eq. (12) this solution can be found in closed form, after straightforward algebra we obtain

$$\theta(\xi) = \arccos\left[1 - \frac{4(1+h)}{2 + h + h\cosh(2\xi\sqrt{1+h})}\right], \quad \xi \geq 0, \tag{14}$$

with $\theta(\xi) = 2\pi - \theta(-\xi)$ for $\xi<0$. In terms of ξ, the boundary condition satisfied by θ in Eq. (14) is, therefore,

$$\theta(+\infty) = 0, \quad \theta(-\infty) = 2\pi. \tag{15}$$

We emphasize that the obtained solution with magnetostatics neglected turns out to be independent of α, which is natural in view of the isotropy of the differential operator in Eq. (12). Thus, for any $h>0$ the 360° domain wall solution has the form of a one-dimensional front whose energy is independent of the wall orientation (see also Refs. 8 and 9). Note that this is very different from the corresponding properties of the Néel walls, which strongly prefer to align along the easy axis.[2,46]

On the other hand, when $h \to 0$ in Eq. (12), the solution given by Eq. (14) transforms into a pair of 180° walls of equal rotation sense separated by a distance of order $O(\ln h^{-1})$ which goes to infinity. Therefore, in the limit there are actually no monotone decreasing solutions of Eq. (12) that satisfy the boundary conditions in Eq. (15). This poses the main difficulty in ascertaining the existence of 360° wall solutions of Eqs. (10) and (11) in the absence of the applied field, since in such a solution the magnetostatic energy has to play a constructive role. In the following we demonstrate that this is indeed the case, at least for certain ranges of parameters.

B. Existence of stable 360° domain walls due to magnetostatics

Even though there are no wall-type solutions to Eq. (12) with $h=0$ satisfying Eq. (15), the discussion above motivates us to look for stationary solutions of Eqs. (10) and (11) with $h=0$ on $\mathbb{R}^2$ which are one dimensional. That is, in terms of the variables of Eq. (13) we will look for a solution θ

$=\theta(\xi)$ which satisfies the conditions at infinity from Eq. (15) for a given α. We note that the idea of a possibility of the existence of a 360° domain wall solution corresponding to $\alpha=\pi/2$ as a local minimizer of the micromagnetic energy functional was first pointed out in Ref. 47.

Substituting the above ansatz into Eqs. (10) and (11) and integrating over $\eta\in\mathbb{R}$, after some algebra we obtain

$$\frac{\partial^2\theta}{\partial\xi^2}-\frac{1}{2}\sin 2\theta-h\sin\theta-\frac{\nu}{2}\cos(\theta-\alpha)\left(-\frac{\partial^2}{\partial\xi^2}\right)^{1/2}\times\sin(\theta-\alpha)=0. \tag{16}$$

Here we introduced the notation

$$\left(-\frac{\partial^2}{\partial\xi^2}\right)^{1/2}v(\xi)=\frac{1}{\pi}\fint_{-\infty}^{+\infty}\frac{v(\xi)-v(\xi')}{(\xi-\xi')^2}d\xi', \tag{17}$$

where $\fint\cdot$ denotes the Cauchy principal value of the integral about $\xi'=\xi$. Once again, this operator is essentially the Dirichlet-to-Neumann operator associated with the Laplacian operator on half-plane,[37] and we have

$$e^{-iq\xi}\left(-\frac{\partial^2}{\partial\xi^2}\right)^{1/2}e^{iq\xi}=|q|. \tag{18}$$

To solve Eq. (16), we studied the time-dependent solutions of Eqs. (10) and (11) restricted to be independent of η. These satisfy the evolution problem

$$\frac{\partial\theta}{\partial t}=\frac{\partial^2\theta}{\partial\xi^2}-\frac{1}{2}\sin 2\theta-h\sin\theta-\frac{\nu}{2}\cos(\theta-\alpha)\times\left(-\frac{\partial^2}{\partial\xi^2}\right)^{1/2}\sin(\theta-\alpha), \tag{19}$$

with boundary conditions from Eq. (15). Note that this evolution equation is a gradient flow generated by the nonlocal energy functional,

$$E[\theta]=\int_{\mathbb{R}}\left\{\frac{1}{2}\theta_\xi^2+\frac{1}{2}\sin^2\theta+h(1-\cos\theta)+\frac{\nu}{4}\sin(\theta-\alpha)\times\left(-\frac{\partial^2}{\partial\xi^2}\right)^{1/2}\sin(\theta-\alpha)\right\}d\xi. \tag{20}$$

As initial data, we chose a profile close to the expected wall profile: $\theta(\xi,0)=2\pi/(1+e^{\xi/2})$.

To solve the time-dependent problem in Eq. (19) with these initial data, we applied a pseudospectral method (see, e.g., Ref. 48) to Eq. (19), i.e., we discretized the problem in space on a uniform grid consisting of 2^m+1 points with step Δx and used fast Fourier transform (more precisely, a fast-Fourier-transform-based cosine transform algorithm, part of the DFFTPACK package obtained from NETLIB) for time stepping of θ, using first-order difference in time for $\partial\theta/\partial t$ with time step Δt. To improve stability, the second-order spatial derivative was treated implicitly. The simulations were run until the steady state was achieved. The obtained semi-implicit scheme was found to be stable for $\Delta x=0.5$ and $\Delta t=0.1$ when $\nu\lesssim 1$, smaller step sizes were found necessary to accurately resolve the solution for larger values of ν. The results were also independently verified, using the optimal grid code developed by us in Ref. 37. The accuracy of the obtained numerical solution for these values of ν was on the order of 10^{-5} with $m=10$.

We ran our simulations for $h=0$ and $0\le\alpha\le\pi/2$ (by the symmetry of the problem the angle α can always be constrained in this range without the loss of generality) and a range of values of $\nu\lesssim 100$. We found that the algorithm converged to a stationary 360° wall profile whenever $\alpha\neq 0$. For $\alpha=0$, on the other hand, the solution evolved into a pair of Néel walls that were slowly drifting away from each other without reaching the steady state. Thus, our numerical results establish the existence of 360° domain wall solutions for not too large values of $\nu>0$ in the absence of the applied field ($h=0$) whenever $\alpha\neq 0$.

C. Properties of 360° domain wall solutions

1. The wall profile

We now discuss the properties of the obtained solutions in more detail. The profiles of θ, as well as the (scaled) stray field h_s and the components $m_\perp$ and $m_\parallel$ of the magnetization vector **m** along the ξ and η axes, respectively, for $\nu=1$ and $h=0$ are presented in Fig. 1. Note that in terms of the Dirichlet-to-Neumann operator, the stray field is defined as[37]

$$h_s=\frac{1}{2}\left(-\frac{\partial^2}{\partial\xi^2}\right)^{1/2}\sin(\theta-\alpha). \tag{21}$$

In the case $\alpha=\pi/2$, shown in Figs. 1(a) and 1(b), the wall consists of a compact core in which the stray field h_s is localized and the angle θ changes almost linearly from 2π to 0. Note that in this case the deviation of the angle from its equilibrium value (0 or 2π) decays exponentially as $|\xi|\to\infty$ independently of ν. This is in contrast to the behavior of the Néel walls which have algebraic far tails.[2,49–51] This can be readily seen from Eq. (16) at $\alpha=\pi/2$, since when, say, $\theta\to 0$ as $\xi\to+\infty$, the factor in front of the nonlocal operator vanishes, and hence the decay is dominated by the balance of the first two terms. Let us also note that the distributions of $m_\perp$ and $m_\parallel$ in this wall are even and odd, respectively.

When the value of α is decreased, the wall profile broadens, and the stray field becomes less localized. This can be seen from Figs. 1(c) and 1(d) which show the solution at $\alpha=\pi/4$. Let us note that the even/odd symmetry in the distributions of $m_\perp$ and $m_\parallel$ is now lost. Also, the decay of θ away from the wall is now algebraic, rather than exponential for $\alpha=\pi/2$, similarly to the case of Néel walls. Finally, when $\alpha\ll\pi/2$, the solution looks like a pair of weakly interacting Néel walls, as can be seen from Figs. 1(e) and 1(f). These walls go further and further apart as $\alpha\to 0$, and there is apparently no 360° wall solution at $\alpha=0$.

The disappearance of the solution as $\alpha\to 0$ can be explained by the following qualitative argument. When $\alpha\ll\pi/2$, the 360° domain wall looks like a pair of 180° degree walls of equal rotation sense separated by a distance exceeding the width of the 180° wall. These two 180° walls interact via two different mechanisms. First, in the absence of magnetostatics the walls would repel each other via exchange interaction (since the latter favors "unwinding" of the twist stored in the 360° wall). On the other hand, the magneto-

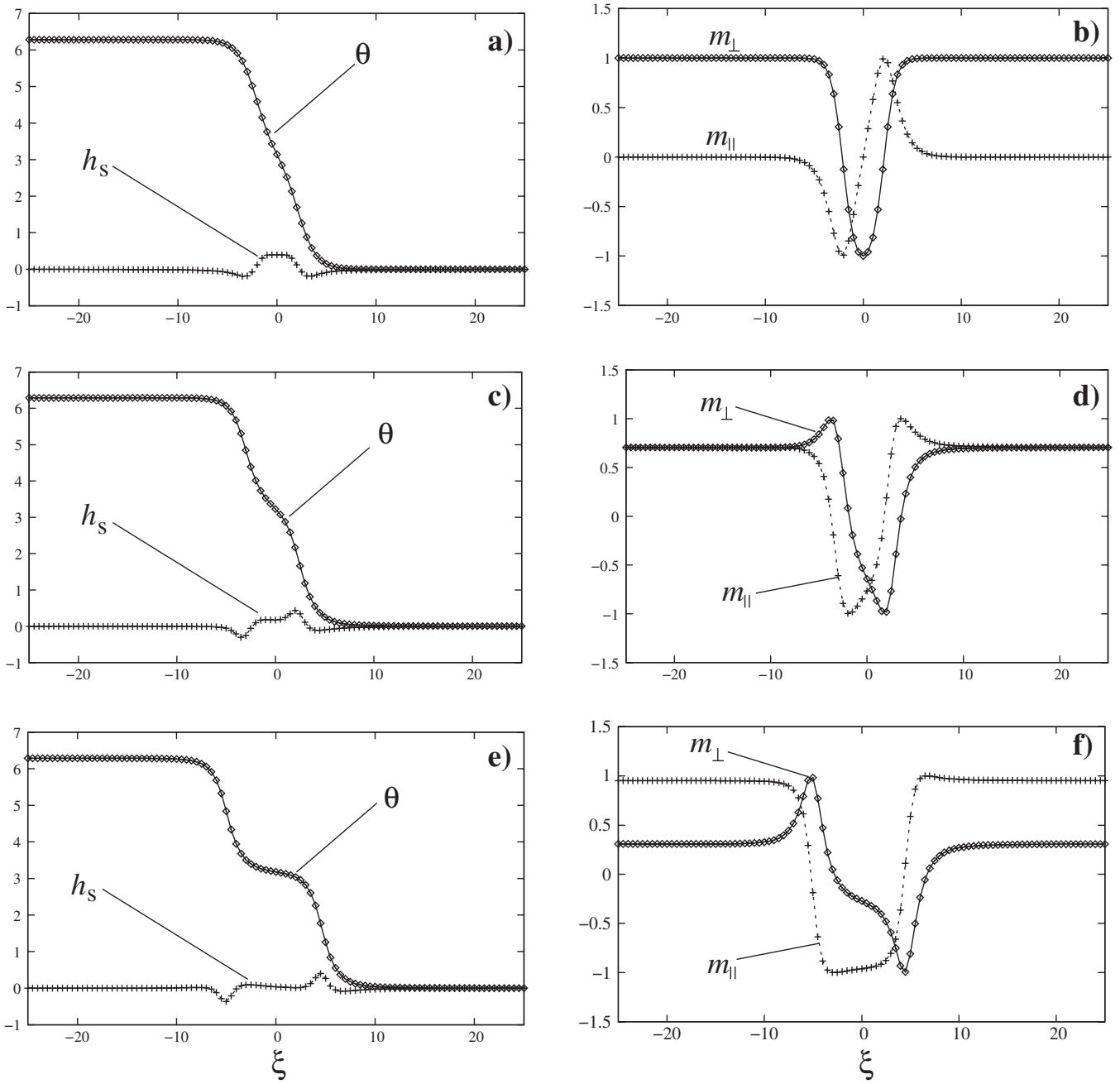

FIG. 1. 360° domain wall solution at $\nu=1$ and $h=0$ for different orientations: $\alpha=\pi/2$ [(a) and (b)]; $\alpha=\pi/4$ [(c) and (d)]; $\alpha=\pi/10$ [(e) and (f)].

static interaction leads to the wall attraction, since for $\alpha\neq 0$ each 180° wall carries an opposite net magnetic charge. It is precisely the competition of these repulsive and attractive forces that makes the 360° domain wall solution stable. Note that this argument also explains why there should not be a stable 360° domain wall solution when $\alpha=0$. In this case each 180° wall (a Néel wall in this case) would only carry a net dipole moment. Moreover, these moments will be opposing each other in each wall, resulting instead in a net repulsion and making the existence of a stable 360° wall impossible. Nevertheless, for any $\alpha\neq 0$ this effect will not play a role, since the dipolar repulsion will decay away faster than the attraction due to net charges, no matter how small those charges actually are.

2. The wall energy

We next investigate the dependence of the wall energy $\gamma(\alpha)$ obtained by evaluating E in Eq. (20) on the solution for a given α and $h=0$. The results for several values of ν are presented in Fig. 2. One can see that for small values of ν the wall energy is essentially independent of the angle α and is equal to roughly twice the Néel wall energy in the absence of stray field. This is also easy to understand, since for small ν the magnetostatic forces act as a perturbation and can be thought of as providing an effective field $h=h_{\text{eff}}$ in Eq. (12). Nevertheless, let us emphasize that the magnetostatic forces are necessary to hold the wall together in the absence of the applied field, and in the case $\nu=0$ the solution disappears.

The dependence of γ on α becomes more pronounced for $\nu\gtrsim 5$, with more anisotropy as the value of ν increases.

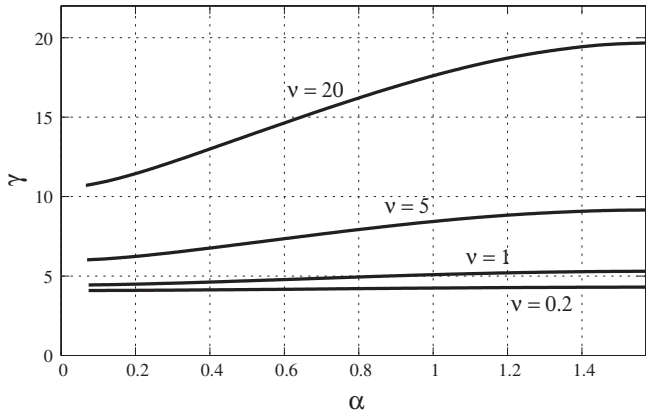

FIG. 2. The dependence of the wall energy γ on α for several values of ν at $h=0$.

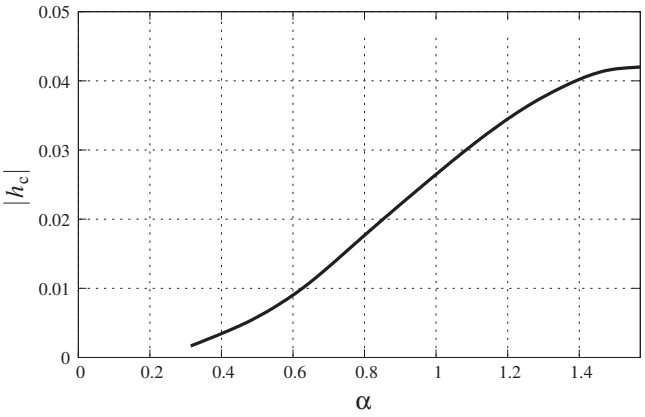

FIG. 3. The coercive field $|h_c|$ of a 360° domain wall at $\nu=1$.

The energy is found to be monotonically increasing in α and, therefore, reaching its maximum at $\alpha=\pi/2$. This should be the consequence of the fact that as α is increased from zero, the magnetic charge in each half of the 360° wall grows, thus increasing the self-interaction energy. Note that in the context of two-dimensional films the wall energy plays the role of the line tension. Thus, in the case of 360° domain walls in the plane we are dealing with problems with anisotropic line tension (see Refs. 52 and 53 for related problems). Let us also note that for fixed ν the dependence of the wall energy on α obtained numerically can be fitted surprisingly well to the following functional form:

$$\gamma(\alpha) \simeq a + b \sin^{3/2} \alpha, \tag{22}$$

where the coefficients a and b depend only on ν. For example, when $\nu=5$, the expression in Eq. (22) agrees with the numerically obtained values to within 1%, if $a=6.0$ and $b=3.2$.

3. Effect of applied field

Finally, we analyzed the effect of an external magnetic field applied in the direction opposite to the direction of magnetization in the periphery of the 360° domain wall. Let us note here that it is clear that if, on the other hand, the field is applied in the direction along the magnetization direction in the periphery of the 360° domain wall, then the wall is further stabilized. This is simply a consequence of the topology of the magnetization in the wall. For this reason, also, the 360° domain wall solution will obviously persist for all $h>0$ in the range of validity of the considered thin film model, even in the absence of magnetostatics, as can be seen from Eq. (12), or when $\alpha=0$. This is also confirmed by the direct numerical solution of Eq. (16).

We found, however, that when the magnetic field is applied in the direction opposite to the direction of the magnetization in the periphery of a 360° domain wall, a critical field strength is required for the wall breakup. Once breakup occurs, the wall splits into two 180° walls moving in the opposite directions, initiating magnetization reversal. To find the value of the coercive field h_c, we performed simulations of Eq. (19) with the same initial data as before and slowly ramping up the intensity of the external field $h<0$ until the wall breaks up at $h=-|h_c|$. The resulting values of $|h_c|$ for different wall orientations and $\nu=1$ are presented in Fig. 3. One can see that the field h_c rather sensitively depends on the angle α and rapidly decreases as α decreases away from $\pi/2$. Let us note that the obtained critical field $|h_c|$ is actually an upper bound for the coercive field of the 360° domain wall in a two-dimensional film, since the breakup of the wall under the action of the reverse field may occur in a two-dimensional manner by, e.g., a corrugation instability of the wall (see also Sec. III G).

D. Variational analysis of 360° domain wall solution

To get a better analytical understanding of the obtained 360° domain wall solutions, we also performed a variational study by minimizing the energy in Eq. (20) over a family of trial functions which resemble the "exact" numerical solution obtained earlier. The family of trial functions was chosen to be given by Eq. (14) with $h=h_{\text{eff}}$, where h_{eff} is now a parameter. This choice is motivated by the fact that the profile in Eq. (14) should be close to the exact solution when $\nu \ll 1$.

To evaluate the energy on a given trial function, it is convenient to use the following alternative representation of the wall energy:

$$E[\theta] = \int_{-\infty}^{+\infty} \left\{ \frac{1}{2}\theta_\xi^2 + \frac{1}{2}\sin^2\theta \right\} d\xi - \frac{\nu}{4\pi} \int_{-\infty}^{+\infty} \int_{-\infty}^{+\infty} \ln|\xi - \xi'| \times \big(\sin(\theta(\xi)-\alpha)\big)' \big(\sin(\theta(\xi')-\alpha)\big)' d\xi d\xi', \tag{23}$$

where $(\cdot)'$ denotes the derivative with respect to the argument of the function in the bracket. For a trial function from Eq. (14) with $h=h_{\text{eff}}$ the first two terms of the energy in Eq. (23) can be computed in closed form. The third term in Eq. (23) cannot be explicitly computed, but is straightforward to evaluate numerically. Combining these results, we obtain that on the chosen trial function,

$$E = 4\sqrt{1+h_{\text{eff}}} + \nu g(h_{\text{eff}}, \alpha), \tag{24}$$

where $g(h_{\text{eff}}, \alpha)$ is the last integral in Eq. (23). We found that $g(h_{\text{eff}}, \alpha)$ is a slowly decreasing function of h_{eff} for fixed α and decreases with α for fixed h_{eff}. In fact, for the relevant range of values of h_{eff} the dependence of $g(h_{\text{eff}}, \alpha)$ on h_{eff} can be very well approximated by the following expression:

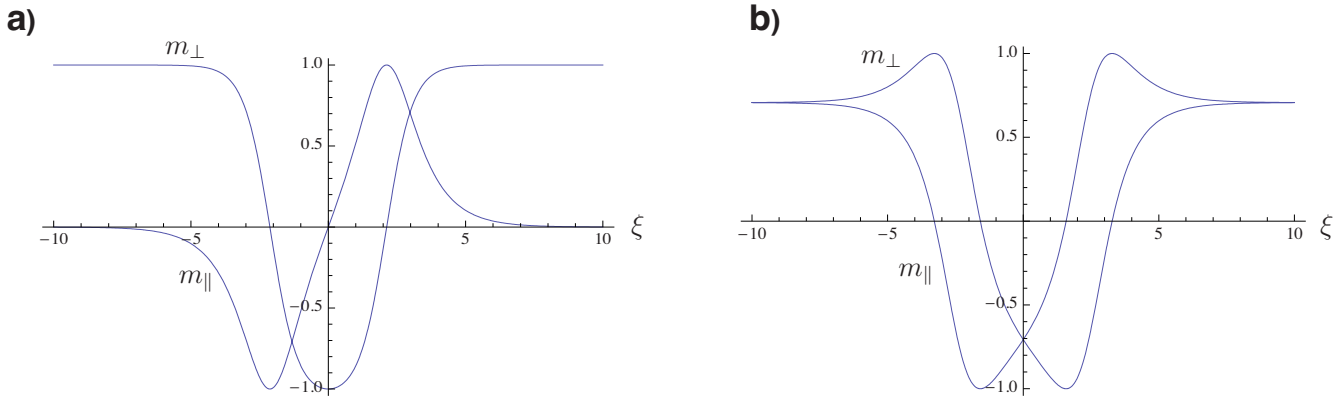

FIG. 4. (Color online) The magnetization in the 360° wall oriented at $\alpha=\pi/2$ (a) and $\alpha=\pi/4$ (b) for $\nu=1$ and $h=0$ obtained from a variational ansatz.

$$g(h_{\text{eff}},\alpha) \simeq 2\pi^{-1}\sin^2\alpha \ln[a \ln(b/h_{\text{eff}})], \tag{25}$$

where the constants a and b depend on α only. This choice of the approximation is motivated by the behavior of the respective integral for $h_{\text{eff}} \ll 1$ and can be shown to be asymptotically exact as $h_{\text{eff}} \to 0$. For example, we found that at $\alpha=\pi/2$ the expression in Eq. (25) with $a=1.4$ and $b=7.2$ approximates the numerically obtained values of the integral for all $h_{\text{eff}} \leq 0.06$ within 1% accuracy. Also note that it is not difficult to see that for $h_{\text{eff}} \gg 1$ we must have $g(h_{\text{eff}},\alpha)=O(1)$.

It is clear from the functional form of Eq. (24) that for every fixed $0<\alpha\leq\pi/2$ and $\nu>0$, there exists a global minimum of E at a particular value of $h_{\text{eff}}>0$. We minimized the expression for E in Eq. (24) at different values of ν and α and compared them to the results of the direct numerical solution. We found good quantitative agreement for all not too large values of ν. Here we present the details of the analysis of the $\nu=1$ case for several values of the wall orientation angle α. Using for simplicity the approximation in Eq. (25) for $\alpha=\pi/2$, we found that the energy E is minimized at $h_{\text{eff}}=0.0714$ and the corresponding energy minimum is $E=5.333$. Similarly, for the case $\alpha=\pi/4$ we have, respectively, $h_{\text{eff}}=0.0318$ and $E=4.936$. We note that the values of E obtained in this way turn out to be within 1% of the values of γ obtained in the simulations of the preceding sections, justifying our choice of the trial functions. We verified that the wall energy obtained by our variational procedure remains accurate within ~10% for $\nu=5$, and the accuracy increases rapidly as ν decreases within the interval $0.2\leq\nu\leq5$ we studied. Also, the resulting profiles of $m_\perp$ and $m_\parallel$ at $\nu=1$ for $\alpha=\pi/2$ and $\alpha=\pi/4$ are shown in Fig. 4. One can see that these profiles are virtually indistinguishable from those shown in Fig. 1.

Finally, let us discuss the behavior of the solution in the case $\alpha \ll \pi/2$. Here one would expect the solution to be close to a pair of Néel walls of the same rotation sense separated by a distance that exceeds the size of the wall core. It is not difficult to see from Eq. (14) that the distance d between these two Néel-like walls can be large only when $h_{\text{eff}} \ll 1$, and we have asymptotically $d=\ln h_{\text{eff}}^{-1}$. Therefore, minimizing the energy in Eq. (24) and using Eq. (25), we find that to the leading order in α we must have

$$h_{\text{eff}} \simeq \frac{\nu\sin^2\alpha}{\pi \ln(\nu^{-1}\sin^{-2}\alpha)}. \tag{26}$$

This allows us to make a qualitative conclusion about the existence of 360° domain wall solutions for all $\alpha>0$ as $\alpha \to 0$, within our choice of the trial function.

E. Stability of 360° domain wall solutions

Let us emphasize that since our 360° domain wall solutions are obtained as long time limits of the evolutions governed by Eq. (19), they must necessarily be stable with respect to one-dimensional perturbations. However, a general analysis of the wall stability with respect to two-dimensional perturbations, which include wall bending, in particular, is complicated because of the presence of nonlocal terms. Nevertheless, one can still draw conclusions about the wall stability with respect to slow transverse modulations, using simple arguments below.

Consider a straight 360° domain wall $\theta=\theta(\xi)$ oriented at angle α with respect to the easy axis, and let us perturb this solution by introducing a transverse displacement $u=u(\eta)$, so that we change $\theta(\xi) \to \theta[\xi-u(\eta)]$. Assuming that u varies slowly with η, we can write down the leading order expression for the wall energy and then Taylor expand it in the powers of $|u_\eta| \ll 1$,

$$E\{\theta[\xi+u(\eta)]\} \simeq \int_0^L \gamma(\alpha+\arctan u_\eta)\sqrt{1+u_\eta^2}\,d\eta$$
$$\simeq \gamma(\alpha)L + \frac{\gamma(\alpha)+\gamma''(\alpha)}{2}\int_0^L u_\eta^2 d\eta, \tag{27}$$

where we assumed that the unperturbed wall has length L and denoted $u_\eta=\partial u/\partial\eta$. From this equation one can see that the wall should be longitudinally stable (at least, for long-wave perturbations) when $\gamma(\alpha)+\gamma''(\alpha)>0$, a well-known result for problems with anisotropic line tension.[52–54] We verified that this condition is indeed satisfied for the 360° domain wall solutions obtained by us for not too big values of ν. Interestingly, we found that as the value of ν is increased, the coefficient in front of the integral in Eq. (27) actually becomes relatively small at $\alpha=\pi/2$ (however, we did not observe a situation in which it changes sign). There-

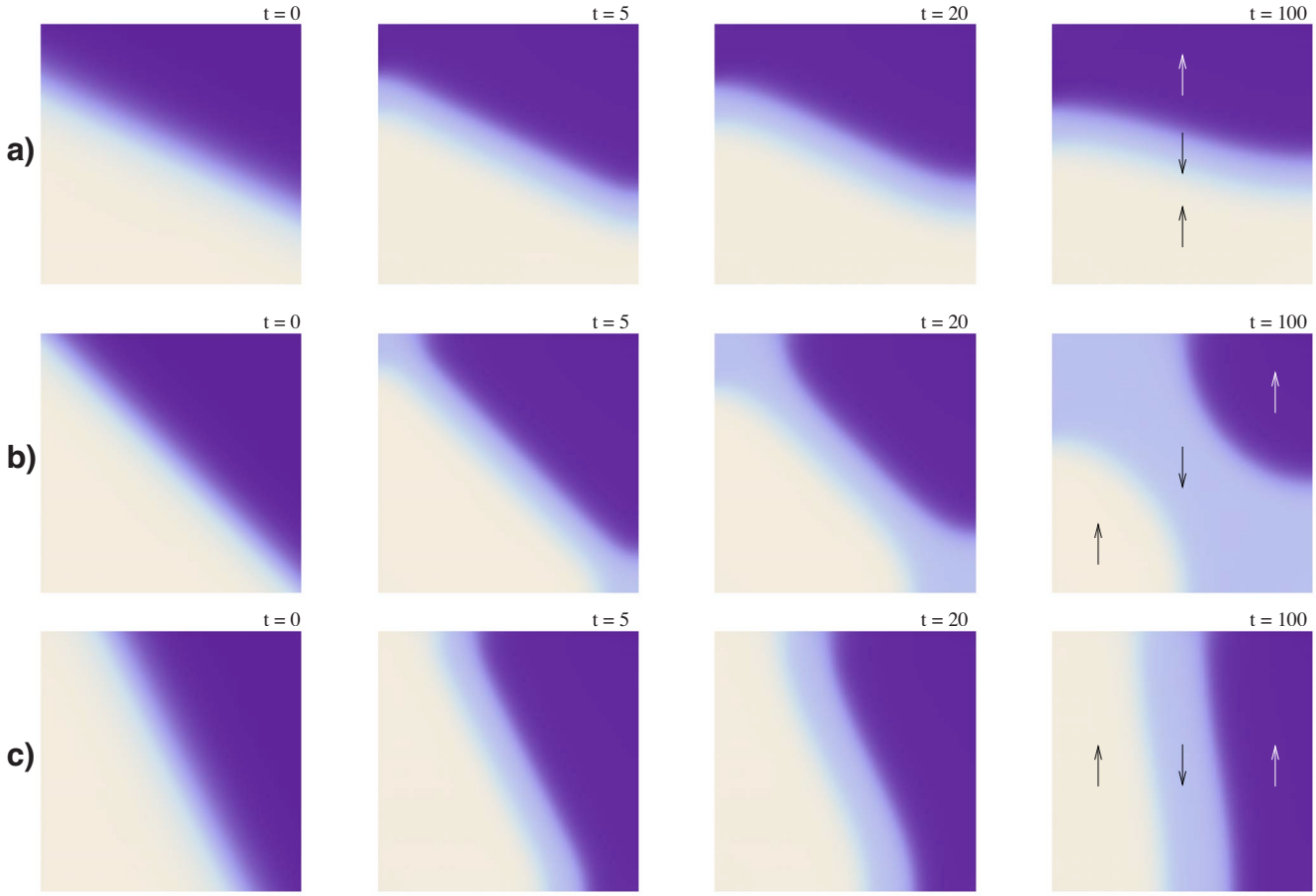

FIG. 5. (Color online) Density plots showing the snapshots of θ at different times in a two-dimensional 32×32 square sample at $\nu=1$ for initial conditions mimicking 360° walls with different orientations. In all simulations the easy axis is vertical. The dark areas are where $\theta\approx0$ and the light areas are where $\theta\approx2\pi$. The arrows indicate the directions of the magnetization corresponding to each area.

fore, we expect that for large enough values of ν the wall may become quite sensitive to shape disturbances or even unstable with respect to transverse deformations (see Ref. 55, for related instability mechanisms).

To further investigate the full two-dimensional stability of the obtained 360° domain wall solutions, we performed two-dimensional simulations of Eqs. (10) and (11) on a finite square-shaped sample, using an algorithm developed by us in Ref. 37. The results of the simulations for the sample of size 32×32 at $\nu=1$ and no applied field, $h=0$, are presented in Fig. 5. These results were obtained using discretization steps $\Delta x=0.5$, $\Delta t=0.05$, and a Zolotarev optimal grid with six nodes in the direction normal to the film whose effective length was $L_z\simeq500$, see Ref. 37, for details. The three different simulations shown in Fig. 5 correspond to different choices of initial conditions for θ. In Fig. 5(a), the initial data are chosen to mimic a 360° domain wall running at an angle $\alpha\approx\pi/3$ to the easy axis (vertical). From these initial data an apparently stable 360° domain wall oriented normally to the easy axis was found to form at the end of the simulation, with the transient governed by curvature-driven domain wall motion (late stages of evolution not shown). This simulation shows that 360° wall solutions can be stable (at least on the time scale of the curvature-driven motion) even in finite ideally homogeneous samples with no applied field.

On the other hand, if the initial data are chosen to be aligned with the diagonal of the square, i.e., if $\alpha=\pi/4$, the dynamics changes qualitatively. While θ adopts a tilted 360° domain wall profile in the film interior, at the corners the wall begins to break up, see Fig. 5(b). As a result, the wall later "unzips" into a pair of Néel walls, which eventually exit the sample, leaving it in a uniformly magnetized downstate (not shown). Yet a different scenario is realized in the third simulation, in which the initial data are oriented at an angle $\alpha\approx\pi/6$ to the easy axis, see Fig. 5(c). As in the simulation of Fig. 5(a), the distribution of θ first adopts a wall-like profile, which then begins to move by mean-curvature flow. However, this motion now results in straightening of the wall along the easy axis. As the dynamics progresses, the wall becomes wider, in agreement with the predictions of the preceding sections, until finally it breaks up into a pair of slowly evolving Néel walls. Once again, at the end of the simulation (not shown) the whole film switches to the uniformly magnetized downstate. In summary, these latter two simulations show several possible mechanisms of 360° domain wall breakup. Nevertheless, in contrast to the second simulation, the wall in the third simulation maintained its integrity until late stages of the dynamics. Thus, even when these walls eventually break up, they can be quite robust during the course of evolution of the magnetization field.

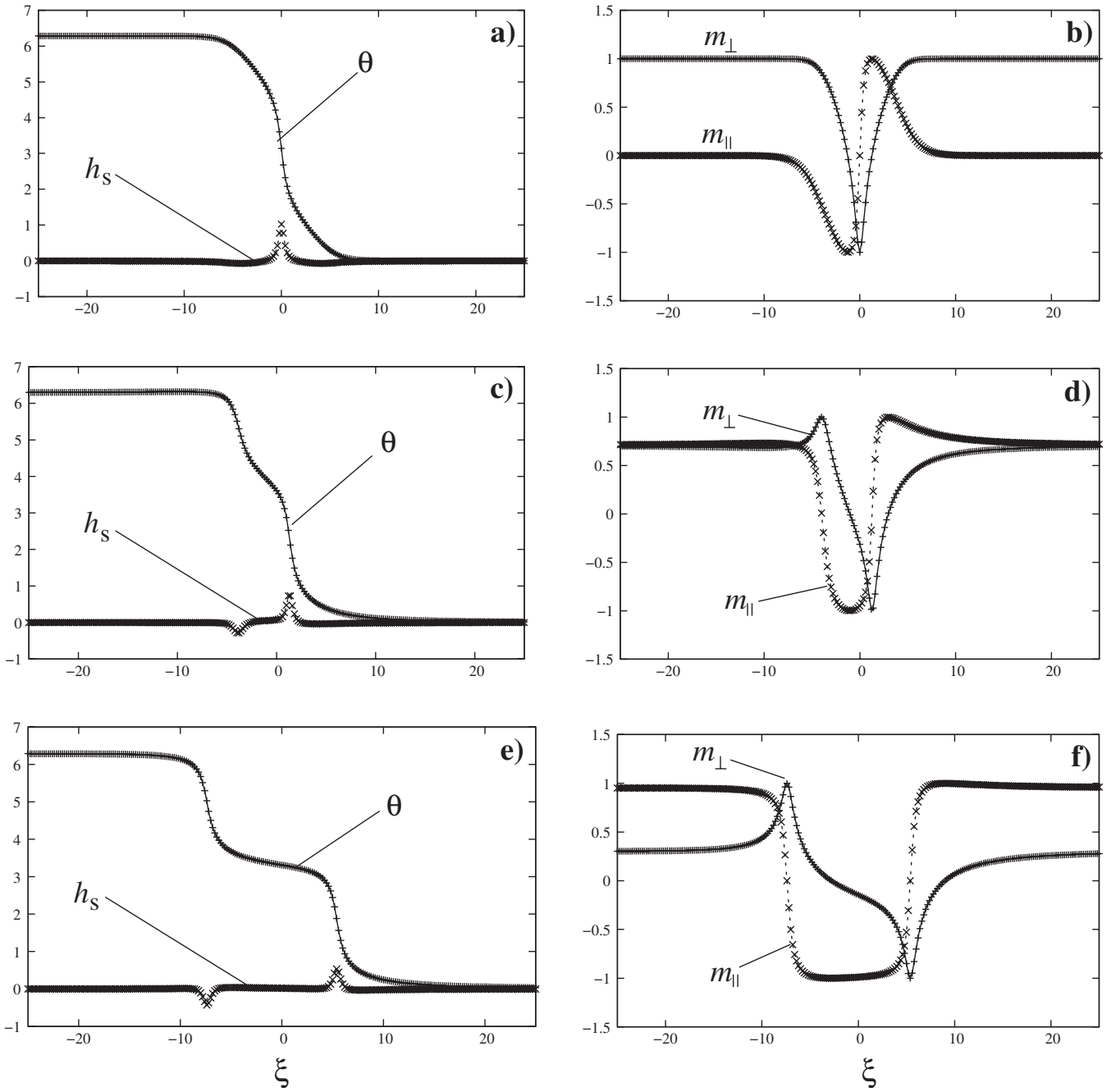

FIG. 6. 360° domain wall solution at $\nu=10$ and $h=0$ for different orientations: $\alpha=\pi/2$ [(a) and (b)]; $\alpha=\pi/4$ [(c) and (d)]; $\alpha=\pi/10$ [(e) and (f)].

F. The case of strong magnetostatics: $\nu \gg 1$

Let us now discuss the situation in which the magnetostatic forces become more pronounced, namely, when the parameter ν characterizing the role of magnetostatics in the film becomes large. We note that this can be the case, if either the film material under consideration is very soft (e.g., permalloy films) or the film is not too thin (e.g., cobalt films mentioned earlier, when the film thickness exceeds, say, 10 nm).

Our numerical analysis of 360° domain wall solutions indicates that these solutions exist and are stable with respect to one-dimensional perturbations for large values of ν as well, we verified the existence of these solutions up to $\nu \simeq 100$. The profiles of the 360° domain wall solutions at $\nu=10$ for several values of α are shown in Fig. 6. These are obtained from the numerical solution of Eq. (19) discretized with $\Delta x=0.2$ and $\Delta t=0.02$. One can see that despite the fact that here the value of ν is an order of magnitude bigger than in the simulations of Fig. 1, the profiles are qualitatively similar to those obtained at $\nu=1$. The main difference is that the stray field h_s is now more localized in the core regions of the wall. From scaling considerations, the width of the field localization, which is determined by the balance of magnetostatic and exchange interactions, must be on the order of $l_{\text{in}} \sim \nu^{-1}$ in our units. On the other hand, outside these regions the stray field is small, and the length scale is determined by the balance of magnetostatics and anisotropy, $l_{\text{out}} \sim \nu$, again, from scaling considerations. Because $l_{\text{out}} \gg l_{\text{in}}$, the wall acquires fat tails, just as in the case of Néel walls in soft materials.[2,49–51]

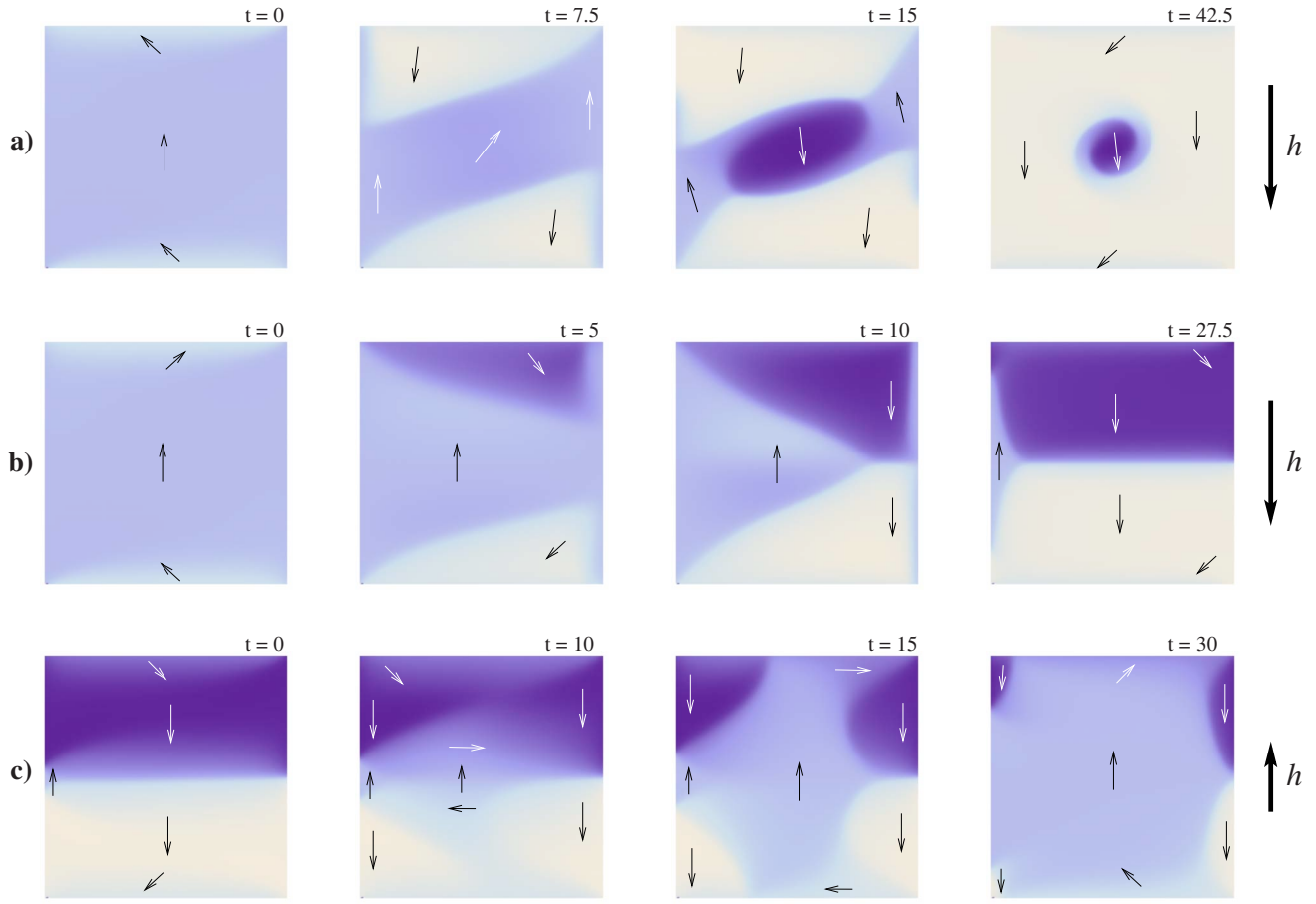

FIG. 7. (Color online) Density plots showing the snapshots of θ at different times in a two-dimensional 32×32 square sample at $\nu=10$ during magnetization reversal, starting from the *S*-state (a), *C*-state (b), and the state with a 360° domain wall (c) [obtained at the end of the simulation in (b)]. The applied field at $t=0$ is $h=-1$ in (a) and (b) and $h=0.2$ in (c). In all simulations the easy axis is vertical. The dark areas are where $\theta\approx-\pi$ the light areas are where $\theta\approx\pi$. The arrows indicate the directions of the magnetization corresponding to each area.

Nevertheless, these solutions may become unstable with respect to transverse perturbations for large enough values of ν, since zigzag wall deformation would decrease the contributions of magnetostatics to the wall energy. To see whether such an instability takes place, we performed two-dimensional simulations analogous to those shown in Fig. 5, but with $\nu=10$. We simulated larger 64×64 samples with discretization steps $\Delta x=0.25$ and $\Delta t=0.0125$; other details of the simulations were as in Fig. 5. We found that all three scenarios of Fig. 5 also persist at $\nu=10$, and these 360° walls are apparently stable with respect to transverse perturbations. We also verified that the same is true for smaller values of ν. Therefore, we expect the obtained 360° domain wall solutions to remain stable in two-dimensional films also for not too large values of ν.

G. Magnetization reversal and 360° domain walls

We also investigated the role which the 360° domain walls might play in the process of magnetization reversal. Figure 7 shows two characteristic scenarios which we observed in our simulations. Here the value of ν was chosen to be sufficiently large ($\nu=10$ in the simulations) in order to observe different well-formed end domains at the top and bottom of the square sample. We first ran the simulation with no applied field to reach a steady state in the form of an *S*-state [Fig. 7(a)] or a *C*-state [Fig. 7(b)]. After the steady state was reached, we switched on the field $h=-1$ in the direction opposite to the overall direction of magnetization in the sample (at the moment marked as $t=0$), mimicking magnetization reversal process by a pulsed field. One can see two very distinct paths the evolution of the magnetization took in the two cases. When the initial state was an *S*-state, the magnetization started to rotate counterclockwise in the end domains and clockwise in the center of the sample. As a result, a 360° domain wall in the form of a loop formed [see Fig. 7(a) at $t=15$; compare also to the experimental observations in Ref. 33]. This wall then shrunk by curvature-driven motion [see Fig. 7(a) at $t=42.5$], until it eventually collapsed and disappeared (not shown). When the applied field was subsequently removed (not shown), the film was left in the *S*-state of opposite polarity.

In contrast, when the field was applied to a sample in the *C*-state, the magnetization in the top end domain began to rotate clockwise, while in the bottom end domain it rotated counterclockwise. As the end domains collided while moving toward each other under the action of the applied field, a horizontal 360° domain wall formed [see Fig. 7(b) at $t=10$]. The wall then "zipped up" across the entire sample [see Fig. 7(b) at $t=27.5$], until eventually no traces of the up domain were left (not shown). When the field was subsequently re-

moved, the 360° domain wall remained in the sample. A finite opposite applied field was then required to remove the wall and bring the sample back to the original *C*-state (not shown).

Let us emphasize an important distinction between the two magnetization reversal paths just described when considering a sequential application of field pulses of opposite polarity. The first path can be termed a symmetric path in the sense that the path that will be taken by the magnetization under the action of the reverse field of the same magnitude and opposite direction after the film was switched to the down *S*-state state will be the mirror image of the first path. In particular, the same critical field will be required to switch the film back. On the other hand, when switching from the *C*-state, a topological defect in the form of a 360° domain wall is created, making the process of magnetization reversal asymmetric. In particular, a smaller field magnitude is necessary to switch the film back to the up state since now the reversal is initiated by the breakup of the 360° domain wall. This is illustrated in Fig. 7(c), where a field $h=0.2$ is applied to the stable configuration containing a 360° domain wall obtained after the field was switched off in the simulation of Fig. 7(b). Note that the field of this magnitude is not sufficient to initiate magnetization reversal of the *C*-state. Eventually, the film returned to the *C*-state of the beginning of the simulation in Fig. 7(b) (not shown). Let us point out that these scenarios were experimentally observed in the studies of magnetic tunnel junction elements.[30] Also note that similar reversal mechanisms for ramped applied fields were observed numerically in Ref. 56.

We further investigated the effect of the sample geometry on magnetization reversal by simulating the process in a rectangular film of size of 32×64 elongated in the direction of the easy axis, see Fig. 8 (other simulation details are the same as above). Here we started the simulation from an *S*-state, yet, in contrast to the simulation in Fig. 7, the magnetization reversal failed to be symmetric once again. After the field $h=-1$ was applied to the film, the magnetization reversal first proceeded as in Fig. 7(a), but then, instead of the 360° domain wall in the form of a closed loop, a pair of 360° domain walls running across the film formed [see Fig. 8(a) at $t=35$]. These walls then started curvature-driven motion, which is considerably slower than the dynamics leading to wall formation. At $t=100$, the field was switched off and the walls were allowed to relax until $t=200$.

At $t=200$ we applied a new pulse of the reverse field [$h=1$ in Fig. 8(b) and $h=0.2$ in Fig. 8(c)] in order to bring the system back to its original *S*-state. In Fig. 8(b), the field intensity was the same as that in Fig. 8(a). One can see that very quickly the 360° domain walls break apart in an "explosive" manner. At the same time, the end domains also invade from top and bottom, colliding with the remnants of the 360° walls. As a result, the system very quickly settles back to the *S*-state, which persists after the applied field is switched off at $t=300$ (not shown).

In Fig. 8(c), on the other hand, the intensity of the applied field was considerably lower than that in Fig. 8(a), resulting in a much slower return to the *S*-state. Here the 360° domain walls break up into pairs of 180° domain walls [Fig. 8(c) at $t=210$], which then curl up [Fig. 8(c) at $t=225$] and then are pushed out of the film [Fig. 8(c) at $t=235$]. Once again, the system settles into the *S*-state after the field is switched off at $t=300$ (not shown).

Finally, we also analyzed the reversal in a rectangular film in the "flower" state, which is realized in 32×64 samples at smaller values of ν. Figure 9 shows a simulation of magnetization reversal under an applied field $h=-1$ for $\nu=5$, starting from a slightly perturbed flower state (other details of the simulations as before). Here, yet again the reversal mechanism is markedly different from the ones observed above. When the field is applied at $t=0$, the end domains begin invading the sample on the sides. At the same time, because of the topological reasons a vertical 360° domain wall forms in the middle of the sample (Fig. 9 at $t=10$). At $t=30$ the two moving 180° domain walls on the sides collide, forming portions of horizontal 360° domain walls, in addition to the trailing vertical 360° walls. This dynamics eventually leads to the collapse of the up domain in the film center, followed by the reconnection of the 360° walls into two disconnected pieces (Fig. 9 at $t=90$). The latter move much slower due to curvature until they exit from the sample (not shown). After the field is subsequently switched off, the sample remains in the flower state of the opposite polarity.

To summarize the results of this section, our simulations showed that 360° domain walls play a crucial role in the process of magnetization reversal in thin ferromagnetic films, even when these films are ideally homogeneous. In particular, slow magnetization dynamics due to the motion of 360° domain walls may introduce history dependence of the magnetization response on a sequential application of demagnetizing fields of finite duration which will manifest itself as nonuniqueness of the observed magnetization patterns for each field cycle. Of course, it is also clear that the process of switching will become even more affected by the dynamics of 360° domain walls in the presence of material imperfections.

IV. CONCLUSIONS

In conclusion, we summarize the results of our analytical and computational investigation of 360° domain walls in thin ferromagnetic films. The analysis was performed, using a reduced micromagnetic model, Eqs. (10) and (11), appropriate for films in which the magnetization distribution is truly two dimensional and in plane. In this model, the film is characterized by only one dimensionless parameter ν, see Eq. (4), which measures the relative strength of the magnetostatic interaction compared to both anisotropy and exchange. In the considered parameter regime all three interactions are assumed to be of comparable strength, which is the case in many thin films of interest to applications.

We now give a résumé of our main findings.

(1) Stable 360° domain wall solutions exist in the model describing extended ideally homogeneous thin uniaxial films even in the absence of the applied magnetic field, at least when the value of ν is not too large, see, e.g., Fig. 1 (more precisely, these solutions exist and are

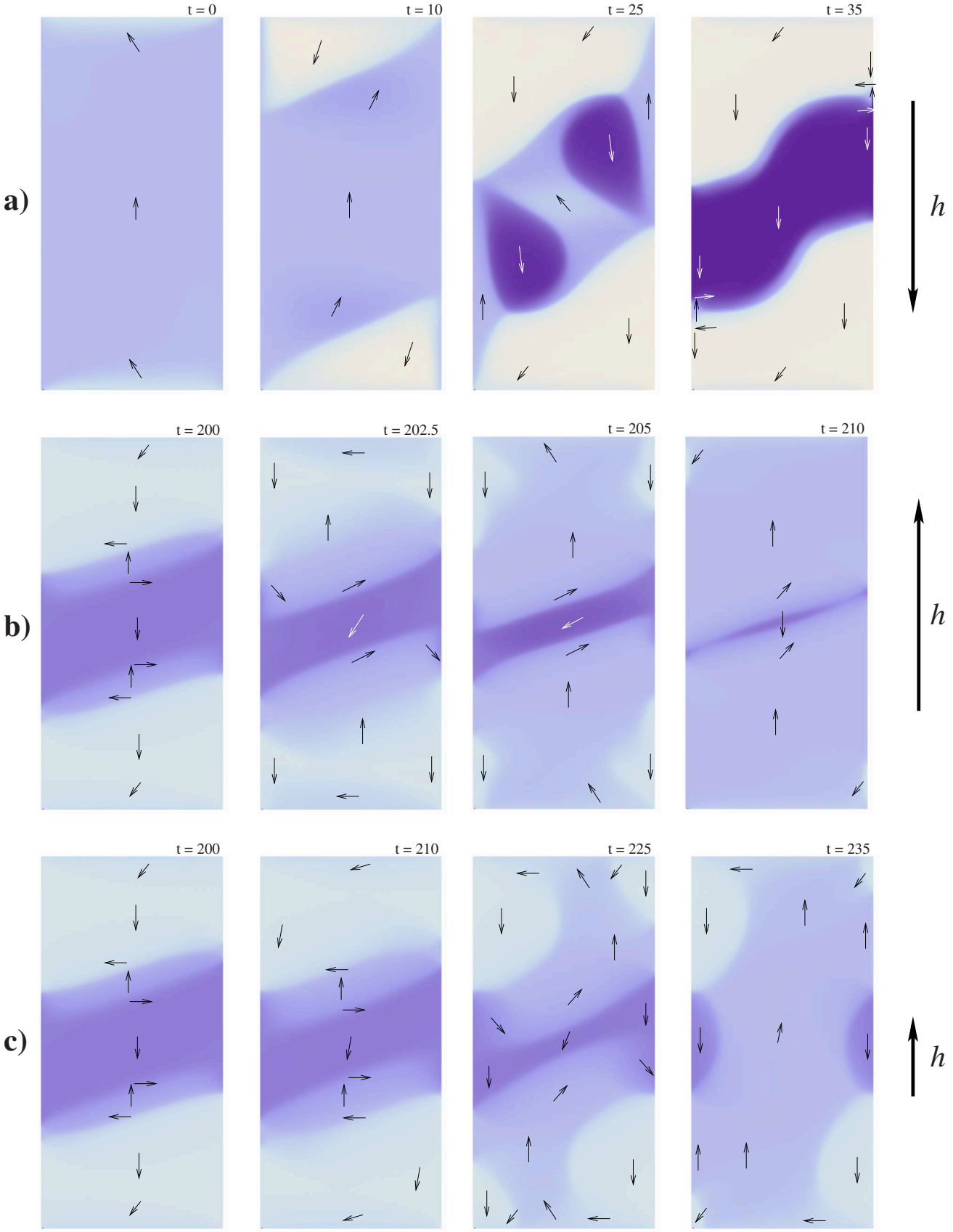

FIG. 8. (Color online) Density plots showing the snapshots of θ at different times in a two-dimensional 32×64 rectangular sample at $\nu=10$ with initial data in the form of an S-state plus a tilted 360° wall. The easy axis is vertical. In (a), the dark areas are where $\theta\approx-\pi$ and the light areas are where $\theta\approx\pi$, in (b) and (c) the dark level of (a) corresponds to $\theta=-2\pi$ and the light level of (a) corresponds to $\theta=2\pi$. The arrows indicate the directions of the magnetization corresponding to each area.

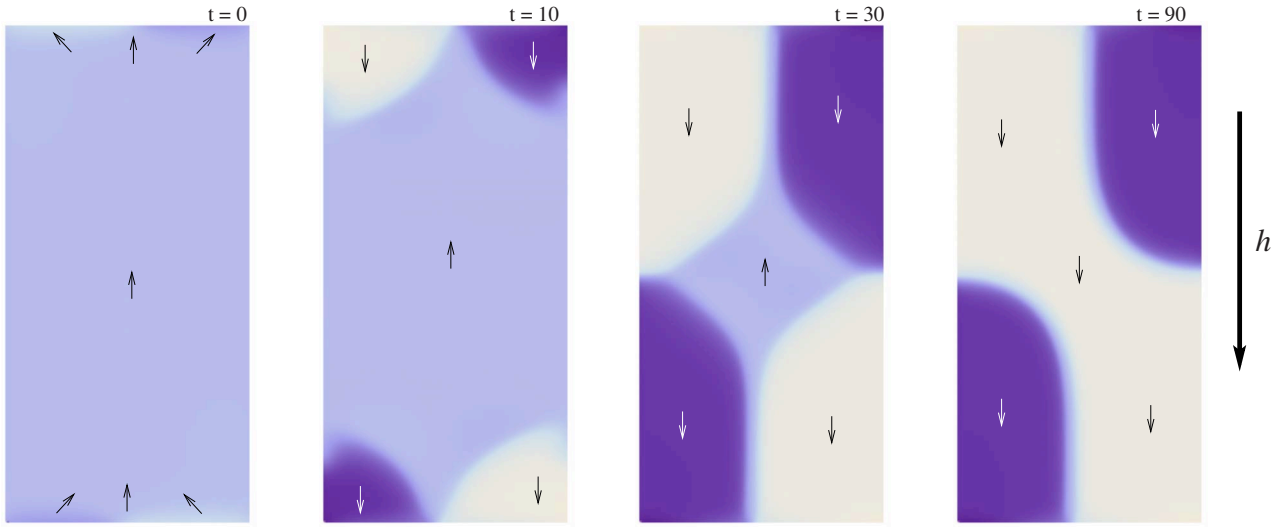

FIG. 9. (Color online) Density plots showing the snapshots of θ at different times in a two-dimensional 32×64 rectangular sample at $\nu=5$ with initial data in the form of a flower state. The easy axis is vertical. The dark areas are where $\theta\approx-\pi$ and the light areas are where $\theta\approx\pi$. The arrows indicate the directions of the magnetization corresponding to each area.

stable as one-dimensional solutions of the reduced micromagnetic equations). However, in order for these solutions to exist, the wall has to be oriented at a nonzero angle α with respect to the easy axis when the applied field is absent. When the magnetostatic interaction is not very strong ($\nu\lesssim 1$), a 360° domain wall solution looks like a bound pair of 180° domain walls of the same rotation sense (see Fig. 1). When the magnetostatic interaction becomes strong ($\nu\gg 1$), the solution becomes a single wall with fat tails, unless the angle $\alpha\ll\pi/2$, when the solution looks like a pair of weakly interacting Néel walls (see Fig. 6).

(2) A 360° domain wall-like distribution of the magnetization which is aligned with the easy axis will always break up into a pair of winding Néel walls which will slowly drift apart in the absence of the applied field. This underscores the anisotropic nature of the 360° domain walls: their energy per unit length γ depends on the wall orientation α and is maximal when the wall is oriented normally to the easy axis (see Fig. 2). This anisotropy is not so significant when the value of ν is not very large, but becomes more pronounced with the increase in ν.

(3) Due to their stability, 360° domain walls may form and remain in an ideally homogeneous film, even though their appearance is often triggered by impurities. Moreover, as we showed numerically, 360° walls, in fact, generically form in finite samples during magnetization reversal even in the absence of any impurities. On the other hand, a finite applied field h_c is necessary to break up a 360° wall into two 180° walls of the same rotation sense. Therefore, 360° domain walls should play a crucial role in the process of magnetization reversal. We found that the critical field for the wall breakup is highest when the wall is perpendicular to the easy axis, making the walls with this orientation most stable with respect to variations in the stray field. However, the critical field needed to break up the wall rapidly decreases as the wall orientation deviates from normal. Therefore, such walls will be more susceptible to variations in the stray field due to boundary effects.

(4) In the context of two-dimensional films, 360° domain walls should be considered as line defects, and so their dynamics is expected to obey the anisotropic mean-curvature flow.[52,53,57] Such motion leads to the wall eventually shrinking to a point and disappearing, or becoming straight, despite the anisotropy in the wall energy.[58] The wall motion, however, will be strongly affected by the dynamics of the domain wall ends. As we showed by our simulations (Fig. 5), when the wall ends reach the boundary of the film which is oriented along the easy axis, the wall becomes asymptotically straight in the direction normal to the easy axis. At the same time, if the wall ends reach the film boundary which is oriented normally to the easy axis, the wall attempts to align with the easy axis, but breaks up in the process, with the resulting Néel walls eventually exiting the sample. Note, however, that the wall ends may also be pinned to inhomogeneities and, therefore, remain immobile.

(5) We demonstrated stability of the 360° domain walls with respect to one-dimension perturbations. It remains to be seen whether these solutions are also stable with respect to transverse perturbations in a two-dimensional film. This analysis is rather involved and goes beyond the scope of the present paper. Nevertheless, our two-dimensional simulations demonstrate transverse stability of the 360° walls for $\nu\lesssim 10$. We also verified that our wall solutions are stable with respect to the long-wave perturbations for all values of ν for which we were able to obtain the solution numerically.

(6) The presence of 360° domain walls may lead to nonuniqueness of the film response to a sequential application of a pulsed magnetic field of finite duration. This has to do with the slow dynamics of the 360° domain walls, once they are formed as a result of the magneti-

zation reversal. Therefore, the domain structures present in the film may be different as each new field pulse arrives, leading to a different reversal path during each cycle. This effect would interfere with the reproducibility of switching under the action of pulsed fields and needs to be taken into consideration in the design of thin film–based micromagnetic devices.

ACKNOWLEDGMENTS

One of us (C.B.M.) would like to acknowledge fruitful discussions with A. Capella, H. Knüpfer, R. V. Kohn, C. Melcher, and M. Novaga. The work of C.B.M. was supported in part by NSF via Grant No. DMS-0718027.

[1]A. Aharoni, *Introduction to the Theory of Ferromagnetism* (Oxford University Press, New York, 1998).
[2]A. Hubert and R. Schäfer, *Magnetic Domains* (Springer, Berlin, 1998).
[3]A. P. Malozemoff and J. C. Slonczewski, *Magnitic Domain Walls in Bubble Materials* (Academic, New York, 1979).
[4]C. L. Dennis, R. P. Borges, L. D. Buda, U. Ebels, J. F. Gregg, M. Hehn, E. Jouguelet, K. Ounadjela, I. Petej, I. L. Prejbeanu, and H. J. Thornton, J. Phys.: Condens. Matter **14**, R1175 (2002).
[5]R. Allenspach, M. Stampanoni, and A. Bischof, Phys. Rev. Lett. **65**, 3344 (1990).
[6]C. Chappert, D. Renard, P. Beauvillain, J. P. Renard, and J. Seiden, J. Magn. Magn. Mater. **54-57**, 795 (1986).
[7]B. Heinrich and J. F. Cochran, Adv. Mater. (Weinheim, Ger.) **42**, 523 (1993).
[8]H. P. Oepen, J. Magn. Magn. Mater. **93**, 116 (1991).
[9]H. P. Oepen, M. Benning, H. Ibach, C. M. Schneider, and J. Kirschner, J. Magn. Magn. Mater. **86**, L137 (1990).
[10]W. H. Rippard and R. A. Buhrman, J. Appl. Phys. **87**, 6490 (2000).
[11]M. Kläui, C. A. F. Vaz, L. Lopez-Diaz, and J. A. C. Bland, J. Phys.: Condens. Matter **15**, R985 (2003).
[12]M. N. Baibich, J. M. Broto, A. Fert, F. N. Van Dau, F. Petroff, P. Eitenne, G. Creuzet, A. Friederich, and J. Chazelas, Phys. Rev. Lett. **61**, 2472 (1988).
[13]G. Binasch, P. Grünberg, F. Saurenbach, and W. Zinn, Phys. Rev. B **39**, 4828 (1989).
[14]T. Miyazaki and N. Tezuka, J. Magn. Magn. Mater. **139**, L231 (1995).
[15]*Ultrathin Magnetic Structures*, edited by B. Heinrich and J. A. C. Bland (Springer, Berlin, 1994).
[16]S. Tehrani, J. M. Slaughter, M. Deherrera, B. N. Engel, N. D. Rizzo, J. Salter, M. Durlam, R. W. Dave, J. Janesky, B. Butcher, K. Smith, and G. Grynkewich, Proc. IEEE **91**, 703 (2003).
[17]J. C. Slonczewski, J. Magn. Magn. Mater. **159**, L1 (1996).
[18]L. Berger, Phys. Rev. B **54**, 9353 (1996).
[19]J. Bass, S. Urazhdin, N. O. Birge, and W. P. Pratt, Phys. Status Solidi A **201**, 1379 (2004).
[20]M. Tsoi, A. G. M. Jansen, J. Bass, W.-C. Chiang, M. Seck, V. Tsoi, and P. Wyder, Phys. Rev. Lett. **80**, 4281 (1998).
[21]E. B. Myers, D. C. Ralph, J. A. Katine, R. N. Louie, and R. A. Buhrman, Science **285**, 867 (1999).
[22]J.-G. Zhu, Y. Zheng, and G. A. Prinz, Science **87**, 6668 (2000).
[23]C. A. F. Vaz, T. J. Hayward, J. Llandro, F. Schackert, D. Morecroft, J. A. C. Bland, M. Kläui, M. Laufenberg, D. Backes, U. Rudiger, F. J. Castano, C. A. Ross, L. J. Heyderman, F. Nolting, A. Locatelli, G. Faini, S. Cherifi, and S. W. Wernsdorfer, J. Phys.: Condens. Matter **19**, 255207 (2007).
[24]F. J. Castaño, C. A. Ross, C. Frandsen, A. Eilez, D. Gil, H. I. Smith, M. Redjdal, and F. B. Humphrey, Phys. Rev. B **67**, 184425 (2003).
[25]F. Q. Zhu, G. W. Chern, O. Tchernyshyov, X. C. Zhu, J. G. Zhu, and C. L. Chien, Phys. Rev. Lett. **96**, 027205 (2006).
[26]D. O. Smith and K. J. Harte, J. Appl. Phys. **33**, 1399 (1962).
[27]R. H. Wade, Philos. Mag. **10**, 49 (1964).
[28]R. H. Wade, Philos. Mag. **12**, 437 (1965).
[29]E. Feldtkeller and W. Liesk, Z. Angew. Phys. **14**, 195 (1962).
[30]X. Portier and A. K. Petford-Long, Appl. Phys. Lett. **76**, 754 (2000).
[31]L. J. Heyderman, H. Niedoba, H. O. Gupta, and I. B. Puchalska, J. Magn. Magn. Mater. **96**, 125 (1991).
[32]M. O. Liedke, K. Potzger, A. H. Bothmer, J. Fassbender, B. Hillebrands, M. Rickart, and P. P. Freitas, J. Appl. Phys. **100**, 043918 (2006).
[33]H. S. Cho, C. Hou, M. Sun, and H. Fujiwara, J. Appl. Phys. **85**, 5160 (1999).
[34]T. Schrefl, J. Fidler, and M. Zehetmayer, J. Appl. Phys. **87**, 5517 (2000).
[35]M. Redjdal, P. W. Gross, A. Kazmi, and F. B. Humphrey, J. Appl. Phys. **85**, 6193 (1999).
[36]D. Ingerman, V. Druskin, and L. Knizhnerman, Commun. Pure Appl. Math. **53**, 1039 (2000).
[37]C. B. Muratov and V. V. Osipov, J. Comput. Phys. **216**, 637 (2006).
[38]T. Trunk, M. Redjdal, A. Kákay, M. F. Ruane, and F. B. Hunphrey, J. Appl. Phys. **89**, 7606 (2001).
[39]C. J. Garcia-Cervera and W. E, J. Appl. Phys. **90**, 370 (2001).
[40]N. Garcia, V. V. Osipov, E. V. Ponizovskaya, and A. del Moral, Phys. Rev. Lett. **86**, 4926 (2001).
[41]R. V. Kohn and V. Slastikov, Proc. R. Soc. London **461**, 143 (2005).
[42]V. A. Molyneux, V. V. Osipov, and E. V. Ponizovskaya, Phys. Rev. B **65**, 184425 (2002).
[43]M. E. Taylor, *Partial Differential Equations II: Qualitative Studies of Linear Equations* (Springer-Verlag, Berlin, 1996).
[44]A. Capella, C. Melcher, and F. Otto, Nonlinearity **20**, 2519 (2007).
[45]N. Ghoussoub and C. Gui, Math. Ann. **311**, 481 (1998).
[46]A. DeSimone, H. Knüpfer, and F. Otto, Calculus Var. Partial Differ. Equ. **27**, 233 (2006).
[47]G. A. Jones and B. K. Middleton, Br. J. Appl. Phys., J. Phys. D **2**, 685 (1969).
[48]B. Fornberg, *A Practical Guide to Pseudospectral Methods* (Cambridge University Press, Cambridge, 1996).
[49]R. Riedel and A. Seeger, Phys. Status Solidi B **46**, 377 (1971).
[50]C. Melcher, Arch. Ration. Mech. Anal. **168**, 83 (2003).
[51]C. J. Garcia-Cervera, Eur. J. Appl. Math. **15**, 451 (2004).
[52]G. B. McFadden, A. A. Wheeler, R. J. Braun, S. R. Coriell, and R. F. Sekerka, Phys. Rev. E **48**, 2016 (1993).
[53]J. E. Taylor and J. W. Cahn, J. Stat. Phys. **77**, 183 (1994).
[54]C. Herring, in *Structure and Properties of Solid Surfaces*, edited by R. Gomer and C. S. Smith (University of Chicago, Chicago, 1952).
[55]C. B. Muratov, Phys. Rev. E **66**, 066108 (2002).
[56]W. Rave and A. Hubert, IEEE Trans. Magn. **36**, 3886 (2000).
[57]F. Almgren, J. E. Taylor, and L. Wang, SIAM J. Control Optim. **31**, 387 (1993).
[58]L. Ambrosio, N. Fusco, and D. Pallara, *Functions of Bounded Variation and Free Discontinuity Problems, Oxford Mathematical Monographs* (Clarendon, New York, 2000).